2012-12-10

Thin Films of Carbon Nanotubes and Nanotube/Polymer Composites

Anthony D. Willey

Brigham Young University - Provo

Thin Films of Carbon Nanotubes and Nanotube/Polymer Composites

Anthony D. Willey

A thesis submitted to the faculty of
Brigham Young University
in partial fulfillment of the requirements for the degree of

Master of Science

Robert Davis, Chair
Richard Vanfleet
David Allred

Department of Physics and Astronomy

Brigham Young University

December 2012

ABSTRACT

Thin Films of Carbon Nanotubes and
Nanotube/Polymer Composites

Anthony D. Willey
Department of Physics and Astronomy, BYU
Master of Science

A method is described for ultrasonically spraying thin films of carbon nanotubes that have been suspended in organic solvents. Nanotubes were sonicated in N-Methyl-2-pyrrolidone or N-Cyclohexyl-2-pyrrolidone and then sprayed onto a heated substrate using an ultrasonic spray nozzle. The solvent quickly evaporated, leaving a thin film of randomly oriented nanotubes. Film thickness was controlled by the spray time and ranged between 200–500 nm, with RMS roughness of about 40 nm. Also described is a method for creating thin (300 nm) conductive freestanding nanotube/polymer composite films by infiltrating sprayed nanotube films with polyimide.

ACKNOWLEDGMENTS

Table of Contents

1. Introduction

Because of their unique electrical properties, thin films of carbon nanotubes (CNTs) have several potential applications in the rapidly growing fields of organic electronics and photovoltaics.[1,2] In organic phovoltaics carbon nanotubes have been used as a semitransparent electrode material, as an electron acceptor material, and as an additive to improve performance of bulk heterojunction solar cells.[3]

There are several ways to create thin films of carbon nanotubes, including filtration of nanotube suspensions,[4] nanotube ink printing,[5] spin casting,[6] and ultrasonic spraying.[7,8] Of these methods, spraying is the most scalable process capable of producing submicron thickness films of carbon nanotubes. The basic ultrasonic spraying process is illustrated in Figure 1, a-b. Current spraying methods require that the nanotubes be suspended by wrapping them in surfactants or long chain polymers that must be removed after spraying, using baths that can easily delaminate the nanotube films from a substrate or harsh nitric acid treatments that can modify the physical and chemical properties of the nanotubes.

Thin film nanotube/polymer composites have many possible applications, one of them being X-ray windows, which require high strength thin films made with low-Z materials. There is an active body of research dedicated to carbon nanotube/polymer composites, much of it focused on exploiting the mechanical, electrical, and thermal properties of nanotubes.[9] Little work, however, has been done on creating submicron thick polyimide composite films with a high weight percentage of carbon nanotubes. Such films can be created by impregnating a nanotube film with a polyimide precursor.[10] In order for the nanotubes to chemically bond with the polyimide, it is necessary to use films of functionalized nanotubes.

1

1.1. Overview

In this thesis I will present a process for spraying carbon nanotubes in which nanotubes are suspended in organic solvents. This process eliminates the need for surfactant removal baths, is compatible with single walled, multiwall, and functionalized nanotubes, and can produce submicron thickness films of randomly oriented nanotubes on a variety of substrates.

I will also present a process for creating thin (300 nm) polyimide/nanotube composite films by spraying nanotubes onto a wafer and then spinning on a polyimide precursor (Figure 1). The films are strong enough to be freestanding, with mechanical properties comparable with pure polyimide. They are also conductive and semitransparent.
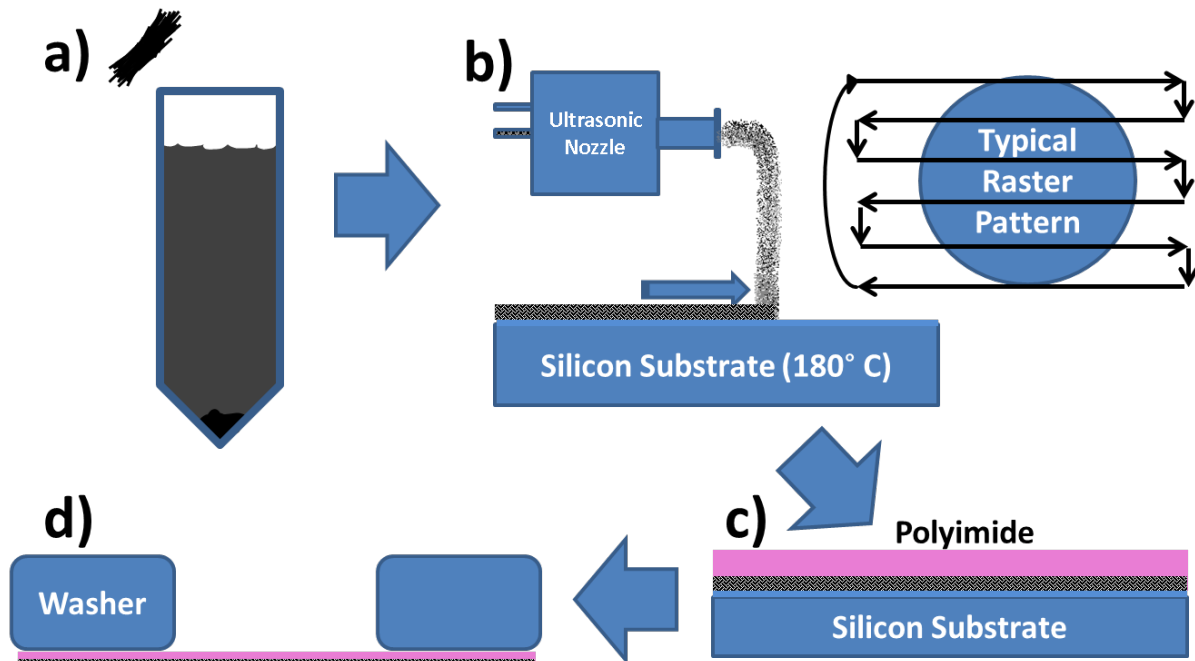
Figure 1: Process schematic: a) Carbon nanotubes are dispersed in a liquid by sonication. b) The nanotube suspension is ultrasonically sprayed onto a heated substrate. c) A polyimide precursor is spun onto the nanotube film. d) The composite film is cured, attached to a metal support ring, and released from the substrate.

Chapter 2 will consist of a brief review of published methods for spraying nanotubes and creating composite films, as well as a short introduction to characterization techniques used in

this work. Chapter 3 will describe in detail the methods for creating and characterizing films. Chapters 4-5 present and discuss the results of the characterization, while Chapter 6 will discuss possible future work, particularly applications in organic electronics and photovoltaics.

2. Background

2.1. Spraying carbon nanotubes

To spray nanotubes, the nanotubes must first be suspended in a solution. This is difficult because nanotubes have strong van der Waals interactions with each other, and consequently form rope-like bundles that impair their conductivity and strength.[11] Nanotube suspension is frequently achieved by covalent functionalization of the nanotubes[7]; however this can be undesirable because functionalization changes the electrical and mechanical properties of tubes.[12]

Surfactants like sodium dodecyl sulfate (SDS), sodium dodecyl benzene sulfonate (SDBS), and Triton-X are frequently used to suspend nanotubes in aqueous solutions[7] without modifying their properties. Alternatively, long chain polymers like sodium carboxymethyl cellulose (CMC) can also suspend nanotubes.[8] The surfactants or polymers are thought to surround or wrap around the nanotubes as they "unzip" from their bundles during sonication.[13]

High quality nanotube films have been created by using an ultrasonic spray nozzle to spray aqueous nanotube suspensions (in SDBS or CMC) onto a heated substrate.[7,8] When sprayed, the solvent evaporates, leaving a film of nanotubes and surfactant. SDBS is removed by soaking the film in a bath of methanol and water to redissolve the surfactant, leaving a film of nanotubes.[7] CMC is removed by soaking the film in nitric acid, removing the polymer and leaving a very smooth (3 nm RMS roughness) collapsed nanotube film.[8]

In my experience, care is required to avoid delaminating the film from the substrate during SDBS surfactant removal baths. Also for some applications, a nitric acid step may have undesirable consequences such as modifying the electronic and optical properties of the nanotubes via carboxylic functionalization and (reversible) HNO_3 intercalation,[14] chemically altering functional groups (e.g. amines) of functionalized nanotubes, or damaging the substrate material. It was to avoid these problems that organic solvents were used to disperse the carbon nanotubes.

 Most organic solvents suspend less than 100 mg of nanotubes per liter of solvent (as opposed to 1000 mg/L for surfactants). N-Methyl-2-pyrollidone (NMP) has been shown to form relatively stable dispersions of individual carbon nanotubes[9, 15] with concentrations around 50 mg/L for single walled tubes, while N-cyclohexyl-2-pyrrolidone (CHP) has been shown to suspend carbon nanotubes with concentrations over 1000 mg/L.[16,17]
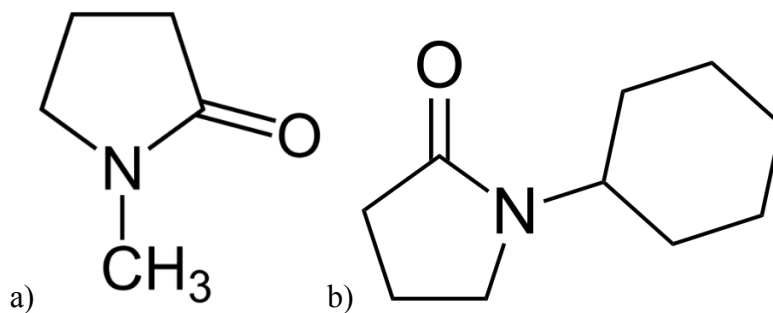

Figure 2: a) N-Methyl-2-pyrrolidone (NMP). b) N-Cyclohexyl-2-pyrrolidone (CHP)

2.2.   Thin nanotube/polyimide composite films

Because of the excellent mechanical and electrical properties of nanotubes, there is an active research effort focused on creating composites of nanotubes and polymers, including

polyimides.[18] There has, however, been little work on creating thin film polyimide composites of submicron thickness with a high weight percentage of carbon nanotubes. Infiltration of single walled nanotubes in polyimide has been reported to increase the hardness and elastic modulus of pristine polyimide thin films.[19] A major challenge with making nanotube composite materials is getting the nanotubes uniformly dispersed in the polymer. This has been achieved in thicker films by using covalently functionalized nanotubes and by suspending nanotubes in organic solvents before mixing them into the polyimide matrix.[20]

Pei et al. (2011) describe a method for creating very thin composite films by mechanically flattening a vertically aligned forest into a dense mat of multiwall nanotubes, spinning on a solution of polyimide precursor, and then curing the polyimide.[10] This resulted in smooth conductive films between about 300–600 nm in thickness that could be suspended on a frame. The films, however, suffered from a high defect density. Specifically, tears were observed in the nanotube films, probably caused by the process of manually flattening (via rolling) the nanotube forest.[10]

2.3.   Characterization techniques

Atomic force microscopy (AFM) is a surface-characterization technique that was developed during the 1980s. An atomic force microscope has a small cantilever with a very sharp tip at the end which is scanned over the surface of a sample using piezoelectric elements. AFM is able to produce high quality images of nanoscale surface morphology.

In scanning electron microscopy (SEM) a focused electron beam is rastered over the surface of a sample. The electrons interact with atoms and electrons in the substrate, emitting secondary electrons, backscattered electrons and X-rays, which can all be detected. Different materials and

geometries eject different numbers and types of electrons, so the detector signal can be combined with the beam position to produce an image of the sample.

A 4-point probe measurement is used for getting conductivity measurements of thin films. Four equally spaced probes arranged in a straight line come in contact with a surface. The outer two probes pass a known current through the film while the inner two probes detect voltage. When the thickness of a film is known and is much smaller than the distance between probes, 4-point measurements can be used to determine the resistivity of material.

An Instron® single column force testing system can be used to test force as a function of extension, and is often used for tension or compression applications. Thin films mounted on small washers can be probed with a rounded tip (see Figure 3), and force vs. extension curves can be obtained with a resolution of millinewtons per micrometer.
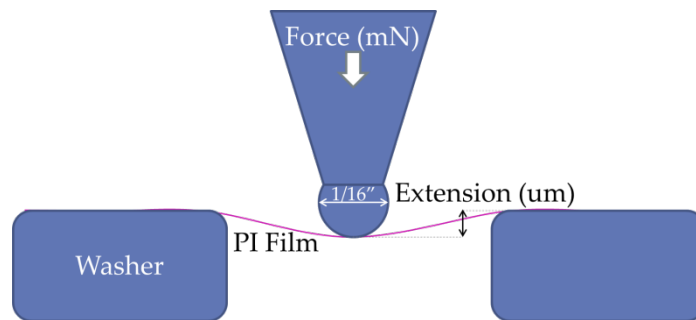

Figure 3: Force test performed by pressing a 1/16" ball bearing into a film suspended on a small washer.

A "bulge" test can be used to determine properties of thin films. In a bulge test, a circular section of thin film is subjected to a pressure differential and the resulting deflection is measured, as shown in Figure 4. The bulge testing equation is given as

$$\frac{Y}{1-v} = \left(P * \frac{r^2}{4dh} - \sigma\right) * \frac{3r^2}{2h^2},$$

Where Y is the Young's modulus, v is the Poisson ratio, P is the pressure differential, σ is the stress, r is the radius, d is the film thickness, and h is the deflection measured at the center.[21]
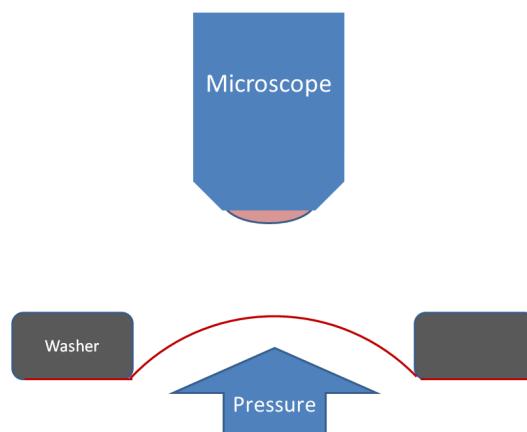
Figure 4: Schematic of a bulge test. A differential pressure was applied under the film and the deflection was measured at the center of the film using a microscope.

3. Methods

3.1. Thin films of carbon nanotubes

Carbon nanotubes were suspended in NMP or CHP and sprayed using an ultrasonic nozzle. The substrate was heated so as to quickly evaporate the solvent and leave a film of randomly oriented nanotubes.

The nanotube suspension was prepared by adding a few milligrams of nanotube powder (SWeNT SG nanotubes from Southwest Nanotechnology) into a beaker containing 100–200 mL of NMP or CHP and then sonicating the mixture for about 20 minutes using a 350 W horn sonicator (Cole Parmer, 0.5 in. tip) with a 50% duty cycle and a power of 40% max power.

(Longer sonication times result in higher concentrations of nanotubes, but with shorter tube lengths.)[7] Concentrations of nanotubes are lower in NMP than in solutions where the nanotubes are suspended via surfactant (less than 0.1 mg/mL, compared to around 1 mg/mL)[16, 22] but sonication resulted in a dark black mixture. After centrifugation at 12,000 RPM (~17,000 g), the supernatant was collected by pipetting the top 75% of solution, being careful to not disturb the pellet of still-bundled nanotubes.

Solution concentration was measured optically. A spectrophotometer was used to perform absorption measurements of a small cuvette of the suspension at 763 nm with an assumed absorption coefficient of 0.043 L/(mg·cm).[11] Typical concentrations ranged from 5-50 mg/L in NMP for single walled nanotubes. Multiwall nanotubes had much higher concentrations; the concentration of SW-100 multiwall nanotubes from Southwest Nanotechnologies was so high that it could not be measured optically.

Solutions were loaded into a syringe pump connected to a Sono-Tek 250 kHz "Impact" ultrasonic spray nozzle. The Sono-Tek nozzle atomizes the liquid while a pressurized airflow directs the droplets down onto a heated substrate. Substrates were typically a silicon wafer or a glass slide, although copper and indium-tin oxide were also used. The hotplate temperature was kept around 180° C for NMP and 200° C for CHP. (NMP boils around 202° C.)

An automated x-y stage was used to raster scan the nozzle over the substrate at a speed of 2.5 cm/s, with a sweep separation of 0.6 cm, and a working distance of 5–8 cm. The nozzle power was 2.5 Watts and the solution was fed to the nozzle with a syringe pump at a flow rate of 0.25 mL/min. The flow rate, temperature, and speed were adjusted so that the solvent evaporated

quickly and didn't stay wet for the next pass. (Higher flow rates can be used with higher temperatures.)

3.2.　　Carbon nanotube/polymer composites

Polymer-nanotube composite films were made by spraying thin (~100 nm) films of nanotubes onto a silicon wafer and then spin coating the films with a layer of polyimide precursor approximately 300 nm in thickness. The polymer solution was a biphenyldianhydride/1,4 phenylenediamine (BPDA/PPD) polyamic acid precursor dissolved in NMP, and was spun on at 2600 RPM for 90 seconds, soft baked at 90° C for about 2 minutes, and then cured at 400° C for 3 hours under argon.

To release the films from the substrate, they were first attached to metal support rings or washers. A spray adhesive was applied to the ring, which was then pressed to the top of the film. The entire structure was then released from the wafer with hydrofluoric acid. The films suspended on washers were then tested mechanically, and were compared to identical polyimide films prepared without nanotubes.

4. Results

4.1.　　Characterization of nanotube films

Sprayed nanotube films ranged from being optically transparent to completely black (see Figure 5). This was controlled by varying the length of the spray time (number of rasters) and the concentration of the suspension being sprayed. The films were mechanically stable, and did not delaminate from the substrate during repeated baths in water and NMP, but could be easily scratched with a pair of tweezers or a razor blade.
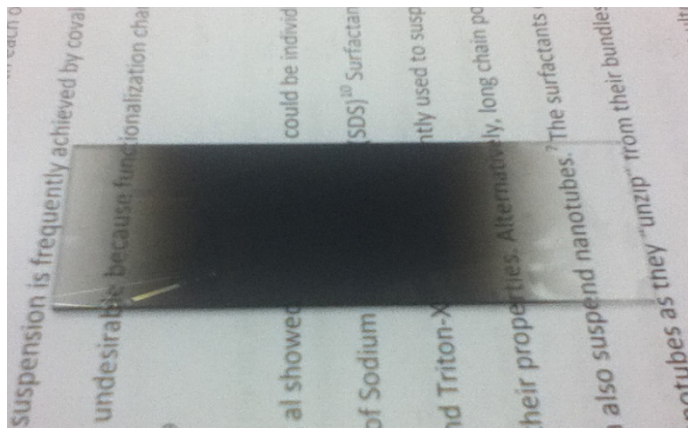
Figure 5: Film of single walled nanotubes sprayed from NMP onto a 3" glass slide. The spray area was 1.5 inches wide, and was covered by repeatedly rastering over the area in 6 sweeps that were 0.25 inches apart. The film is thick enough to be black in the spray area, but becomes transparent as it thins near the edges.

Characterization of the sprayed CNT films was performed using scanning electron microscopy (SEM) and atomic force microscopy (AFM). SEM images showed that the nanotubes were randomly oriented, forming a uniform carpet (see Figure 6). Film thickness was measured by gently scratching a film and then measuring the edge with AFM. Film thickness ranged from about 200 nm to over one micron, and could be controlled by the number of rasters (see Figure 7).

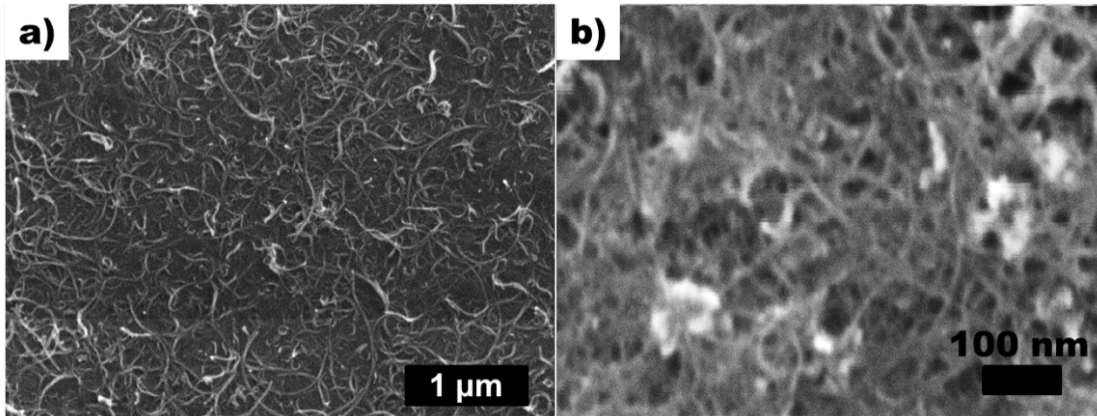Figure 6: SEM images of nanotube films sprayed with NMP. a) A film of amine-functionalized multiwall nanotubes. b) A film of (6,5) single walled nanotubes.
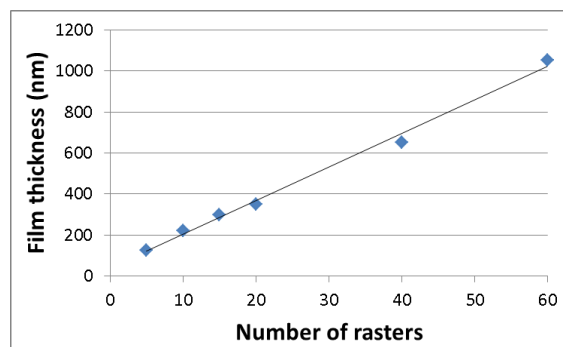
Figure 7: Thicknesses of several multiwall nanotube films, as measured by AFM, plotted as a function of spray time (number of rasters over the spray area)

Because nanotube concentrations are very dilute in organic solvents, one challenge with making films by evaporating the solvent is that any impurities native to the solvent or nanotubes (or that are introduced during processing) remain on the substrate. These impurities showed up under SEM as dark splotches (often forming circular ring patterns, presumably at droplet edges (Figure 8 a). These splotches were not observed when spraying highly concentrated solutions of SWeNT SMW100 multiwall nanotubes, but became clearly evident when spraying less concentrated

11

solutions of single walled nanotubes. It was confirmed by AFM that these "coffee stains" were

actually raised rings of material (see Figure 9).

Figure 8: SEM images of CHP-sprayed films: a) to c) show a film at different magnifications before being washed in NMP, d) to f) show a film after being washed in NMP.
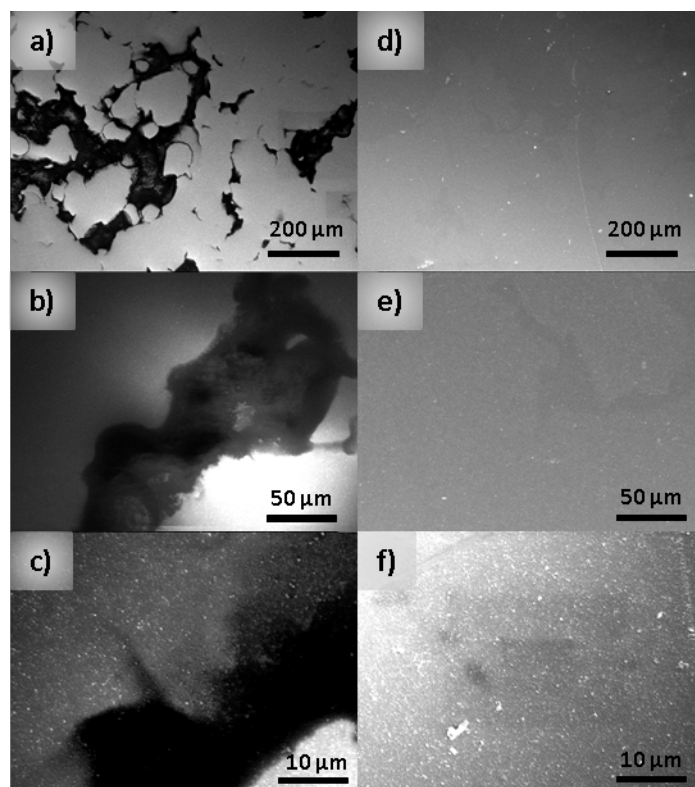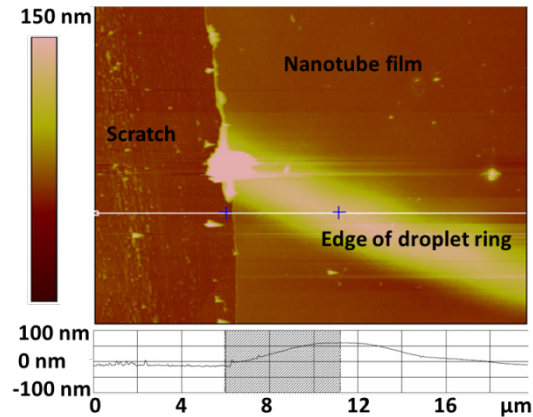
Figure 9: AFM image showing height of a droplet ring resulting from sprayed NMP. The film was scratched with a pair of tweezers on the left.

Because the impurities had come from evaporating NMP, the wafers were dipped in a hot bath of NMP in an attempt to redissolve the impurities. Subsequent AFM and SEM images showed that the nanotubes had been cleaned up significantly (see Figure 8 d). The rings were gone, and the nanotube films looked much cleaner. Similar results were achieved by soaking the film in hot water for an hour.

Energy-dispersive X-ray spectroscopy (EDS) analysis of the rings before the wash and of the nanotube film after the wash showed that the rings were composed, at least in part, of a molybdenum containing compound (Figure 10) that was likely native to the nanotubes. (The nanotubes were Southwest Nanotechnology CoMoCAT tubes, grown from a molybdenum-stabilized cobalt catalyst.)

13
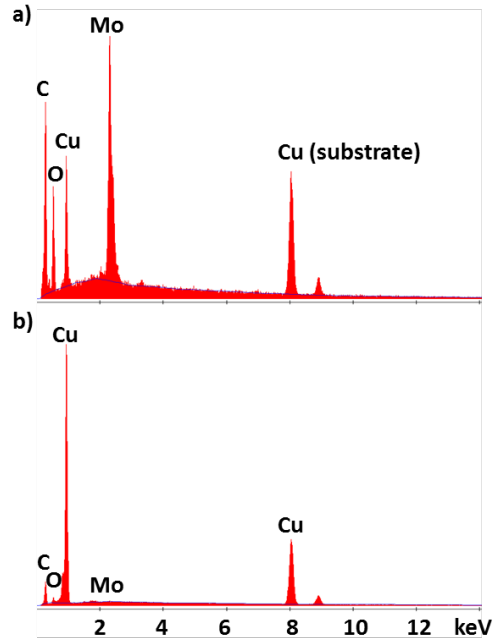
Figure 10: a). EDS of dark splotches showing molybdenum peak; b). EDS of identical film after washing. These films were sprayed on a copper substrate (something that would have been impossible with the nitric acid process).

Figure 11 shows atomic percentages of selected elements from three EDS measurements. The first measurement was of an unwashed sample where the beam was focused on a nanotube-rich region. The second measurement was focused on a dark region, and the third measurement was focused on a large area of the film after it had been washed and the dark splotches had disappeared.
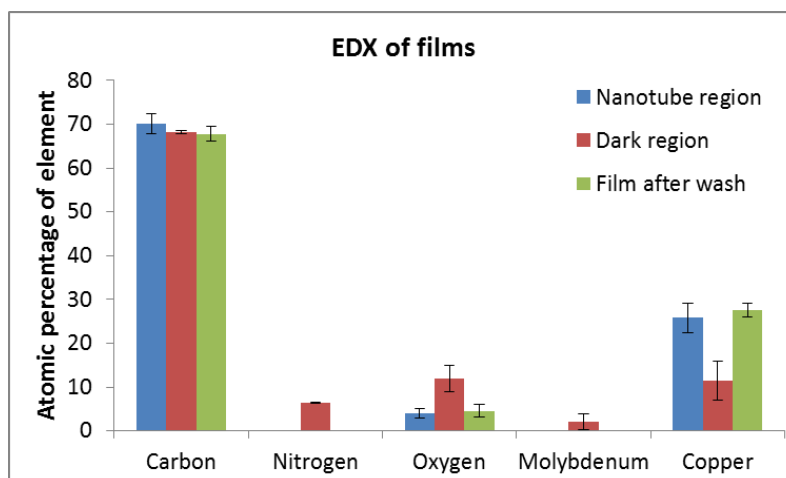
Figure 11: Semi-quantitative analysis showing atomic percentages of elements detected using EDS.

The first and third measurements are similar, showing roughly equal peaks for carbon (from the carbon nanotubes), oxygen (possibly from copper oxide), and copper from the underlying substrate. The second measurement shows new nitrogen and molybdenum peaks, as well as an increased oxygen peak, suggesting that the splotch material was some combination of compounds containing molybdenum, oxygen, nitrogen, and possibly some carbon.

Film resistance measured by a 4-point probe showed sheet resistances ranging from $2x10^3$ to $6x10^3$ Ω/square, and resistivities of around 0.1 Ω·cm, well within the semiconductor range.[23]

AFM measurements (see Figure 12) of film thickness and roughness for several films are shown in Figure 13. The roughness of these films ranged from 10–50 nm which was comparable with some of the previously published films sprayed from SDBS surfactant dispersions[7] but not as smooth as films sprayed from CMC dispersions followed by a nitric acid rinse.[8]
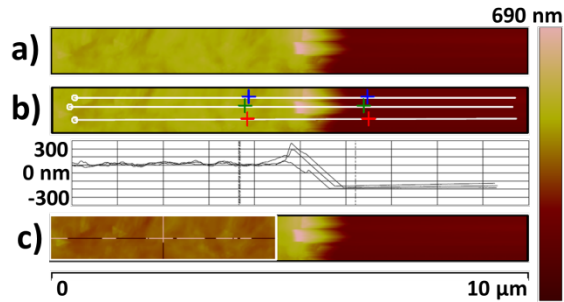
Figure 12: Typical AFM measurements showing a) a scratched nanotube film (nanotubes on the left, scratch on the right); b) the thickness of the film, taken as the average difference of three traces; c) the roughness of the nanotube portion of the same film (measured only on the left)
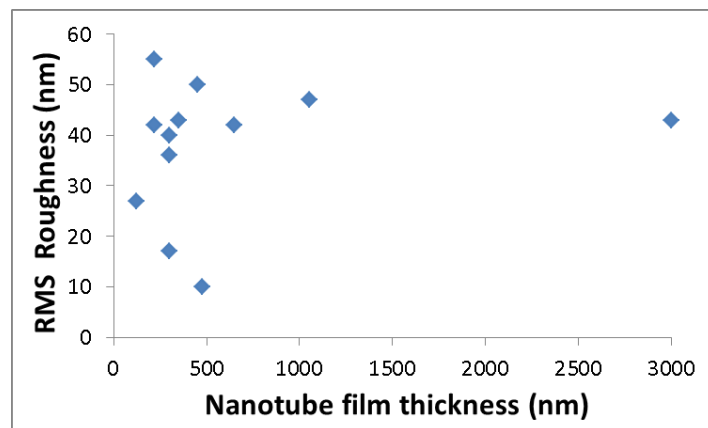
Figure 13: RMS roughness versus thickness of several nanotube films measured by AFM

4.2.   Characterization of CNT/Polyimide composite films

Torn sections of the nanotube-infused polymer films were imaged by SEM, confirming that

nanotubes were infused in the polymer as shown in Figure 14.
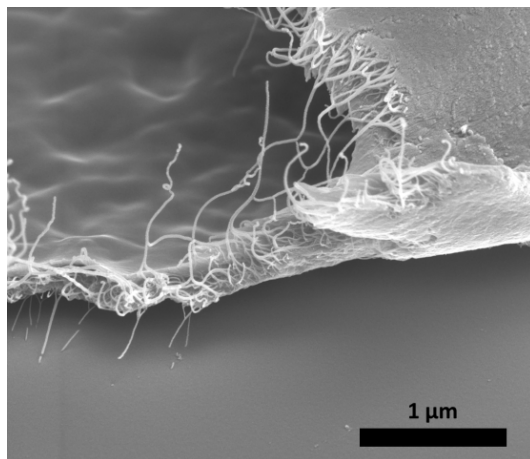
Figure 14: SEM image of a MWNT film that has been infiltrated with a polymer and then torn. Multiwall nanotubes are seen protruding from the bottom portion of the film.

To test the strength of the nanotube/polyimide composite films, several were mounted on 1/8" inner-diameter washers and broken using a 1/16" steel ball bearing attached to a pressure sensor.

The films varied widely in the ultimate breaking force, which seemed to depend more on the thickness of the film than whether or not the film had nanotubes infused in it. Films with thicker layers of nanotubes infused tended to break at lower forces, as in Figure 15, b. Films were created and tested using both single-walled and COOH and Amine functionalized multiwall nanotubes obtained from Cheap Tubes, Inc.
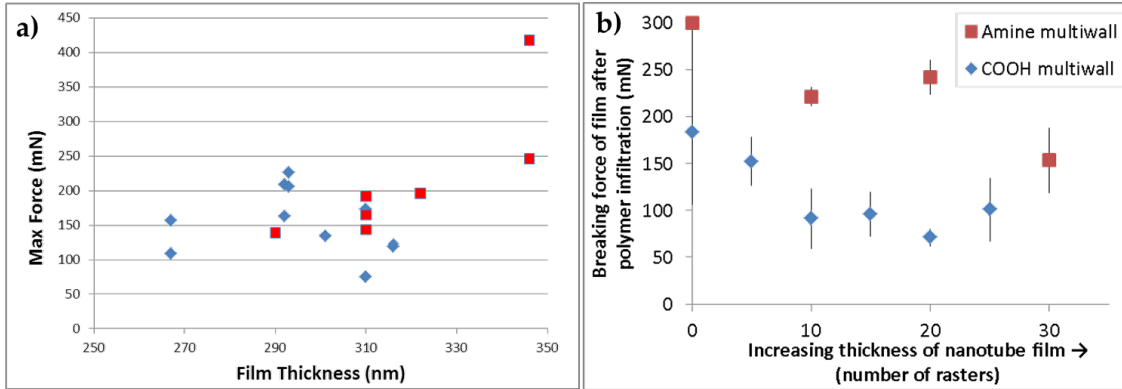
Figure 15: Results of force testing. a) Several tests of a ~100 nm SWNT film impregnated with polyimide. Breaking force is plotted versus total film thickness. Films with nanotubes are fairly indistinguishable from films without nanotubes. b) Breaking force of MWNT films vs. thickness of nanotube layer. The first data points on the left are pure polyimide films with no nanotubes, and the CNT layer thickness was varied by increasing the number of rasters over the substrate for each subsequent sample. Vertical lines represent the standard deviation of several pressure tests on each sample.

"Bulge" tests (Figure 4) were used to quantify the stiffness of the washer-mounted films. A differential pressure was applied on one side of the washer and the deflection at the center of the film was measured with a microscope. For small deflections the Young's Modulus Y is given by:

$$\frac{Y}{1-v} = \left(P * \frac{r^2}{4dh} - \sigma \right) * \frac{3r^2}{2h^2},$$

where v is the Poisson ratio (assumed to be 0.3), P is the pressure differential, σ is the stress, r is the radius, d is the film thickness, and h is the deflection measured at the center.[21] The deflection data for a range of different pressures were fitted with a 3rd order polynomial (see Appendix 1) to obtain experimental values for Young's Modulus. Values of Young's modulus ranged from about 2–3 gigapascals for films, regardless of whether or not they had nanotubes in them.

18
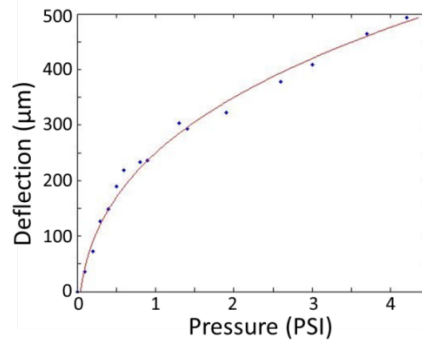
Figure 16: Typical pressure data with a best
fit.

The Matlab program used for fitting the curves is given in Appendix 2.

4.2.1. Electrical characterization

The films retained a lateral electrical conductivity slightly lower than the nanotube films prior to

polymer infiltration. The resistance was measured with a 4-point probe, and sheet resistances

ranged from $2x10^3$ to $6x10^3$ $\Omega/\square$ for single-walled nanotubes. When multiplied by the film

thickness this gives a bulk resistivity on the order of about 1.4 $\Omega \cdot$cm. This falls well within the

range of semiconductor resistivities (about 10^{-4} for heavily doped to 10^6 for intrinsic)[23].

Vertical conductivity was measured by spraying nanotubes and infiltrating polymer on

conductive substrates (initially copper, then indium-tin oxide on glass) and then dabbing silver

epoxy on the top of the film (see Figure 17). The resistance was then measured between the

bottom conductive layer and the top silver epoxy layer.

Figure 17: Silver epoxy dabbed on a
polyimide/nanotube film on ITO glass

Resistance varied based on the film, but the resistance was generally very high, as would be
expected for a thin film of nonconducting polymer. This was because the polymer completely
covered the nanotube film beneath (see Figure 14). These results were consistent even for very
thick nanotube films with very thin polymer films spun on them.

To make the films conductive from top to bottom, they were placed in a Harrick plasma cleaner
(model PDC-001) on high power to etch back the top layer of polyimide precursor. (This was
done before curing the polyimide.)

The etch rate was determined experimentally by spinning a 150 nm layer of polyimide onto a
wafer, cleaving the wafer in half, and then placing one half of the wafer in the plasma cleaner for
5 minute increments.

The color of each film depended on its thickness according to the thin-film-interference equation
$2nd = m\lambda$, where n is the index of refraction in of the film, d is the thickness, λ is the
wavelength of light, and m is an integer. Each film was matched to a standard color chart for

silicon dioxide, and the resulting thicknesses were multiplied by a constant to account for the difference between the indexes of refraction for SiO_2 and polyimide. The constant was determined by dividing the initial polyimide thickness (150 nm) by the thickness of yellowish gold silicon dioxide (200 nm). A plot of the film thickness vs. etch time is shown in Figure 18 h). The etch rate was determined to be approximately 3.2 nm/min.
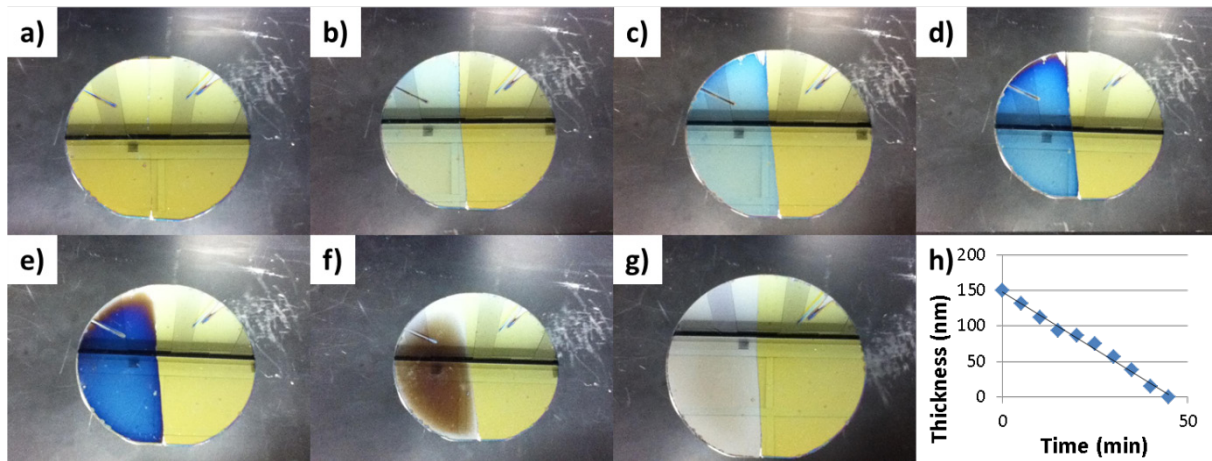
Figure 18: a–g) A silicon wafer with 150 nm of polyimide spun on was split in half and the left side was repeatedly etched for 5 minute increments, while the right side was saved for comparison. h) The resulting film thickness plotted as a function of etch time.

For a given film the appropriate etch time could be determined by subtracting the nanotube film thickness (before polyimide was spun on) from the total film thickness after polyimide was spun on. Plasma etch times were adjusted so as to barely etch into the nanotube layer.

Resistance measurements were performed again between the top and bottom of the film, and the resistance was much lower after the film had been etched and the nanotubes exposed. Figure 19 shows a collection of I-V curves obtained from a 450 nm nanotube film sprayed onto a thin copper foil, coated with approximate 150 nm of polyimide precursor and then etched for 32 minutes. Results from a film sprayed on ITO are shown in Figure 20.
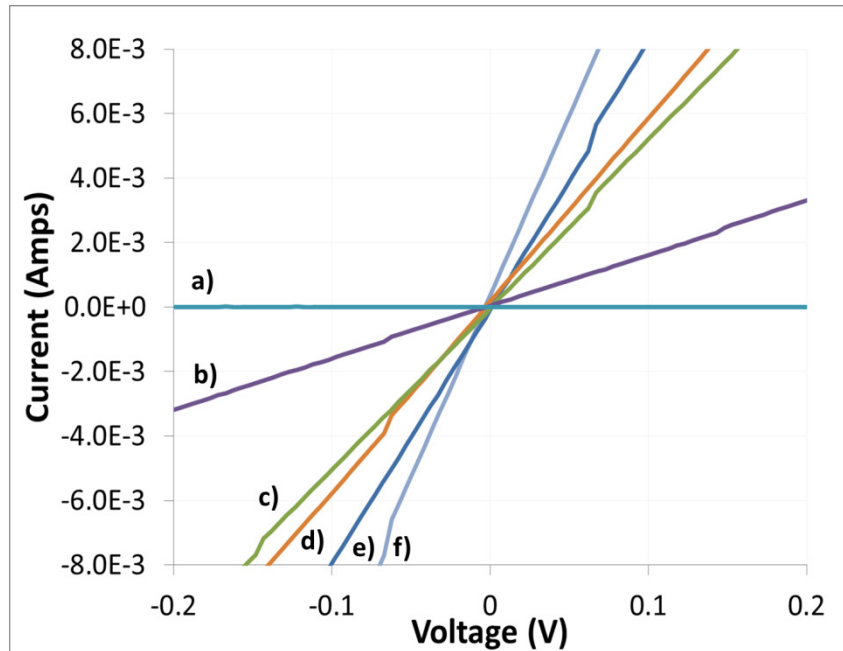
Figure 19: Current-voltage curves showing vertical conductivity in composite films, taken between the underlying copper substrate and a dab of silver epoxy on top. Ordered from least conductive to most conductive are: a) a 450 nm of (6,5) nanotubes with 150 nm of polyimide spun on; b) the same film after etching 40 nm from the top of the film; c) the same film after etching a total of 100 nm from the topof the film; d) the nanotube film before any polyimide was spun on; e) silver epoxy on copper with no film inbetween; f) straight copper with no silver epoxy.

Etched samples were imaged by SEM to verify that nanotubes were being exposed. Resolution between nanotubes and polymer is generally low, but Figure 21 shows bright specks scattered across the surface of the polyimide film. These specks are believed to be the sharp points of nanotubes poking through the surface of the etched polyimide film, suggesting that the nanotubes, as well as the polyimide, were etched by the plasma. In fact, when a film was accidentally left in the plasma etcher for too long, only debris showed up on the SEM.
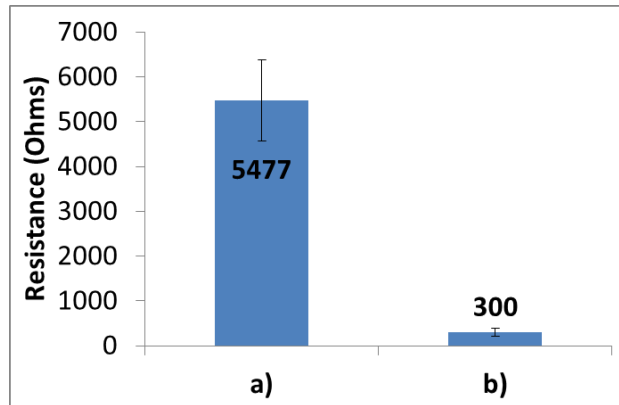
Figure 20: a) Resistance between silver epoxy and ITO before etching back the polyimide b) Resistance after etching back the polyimide
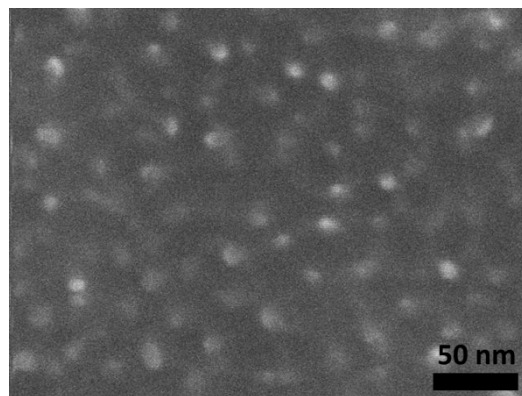
Figure 21: SEM image of nanotube/polyimide film that has been etched back to expose the nanotubes.

5. Discussion

5.1. Nanotube films

Spraying nanotubes suspended in organic solvents eliminates the need for surfactant or polymer wrapping, and produces thin films of randomly oriented nanotubes. An advantage to this method

23

is that it doesn't require a surfactant-removal bath, during which the film is sensitive to disturbances that can damage the film. Also, in the case of CMC-suspended tubes, it avoids the nitric acid step.   Drawbacks would in some cases include spraying at high temperatures of >180 °C, and longer spray times because of low nanotube concentration. The resulting films can readily be infiltrated with polyimide, producing freestanding conductive polymer films, with strength comparable to the original polyimide. The technique is compatible with single walled nanotubes, multiwall nanotubes, and multiwall functionalized nanotubes.

5.2.   Polyimide composites

Instead of growing and rolling nanotube films as described by Pei et al., I have used the methods in Section 3.1 to spray carbon nanotube films. I then followed a procedure similar to that described by Pei et al. to infiltrate the films with a polyimide precursor, cure the polyimide, and release it from the substrate. These thin conductive films showed improved mechanical properties compared to the rolled nanotube films, and were comparable with films made of straight polyimide.

6. Future work

 The field of organic photovoltaic devices (OPVs) has expanded rapidly over the past 20 years and several efficiency records have recently been broken by polymer-fullerene devices.[24] Figure 22 shows exponential growth in the number of publications per year contributing to the subject of "polymer solar cell(s)." While OPVs offer promising alternatives to traditional Silicon solar cells, efficiencies of current devices are still too low (<10%) to compete economically.
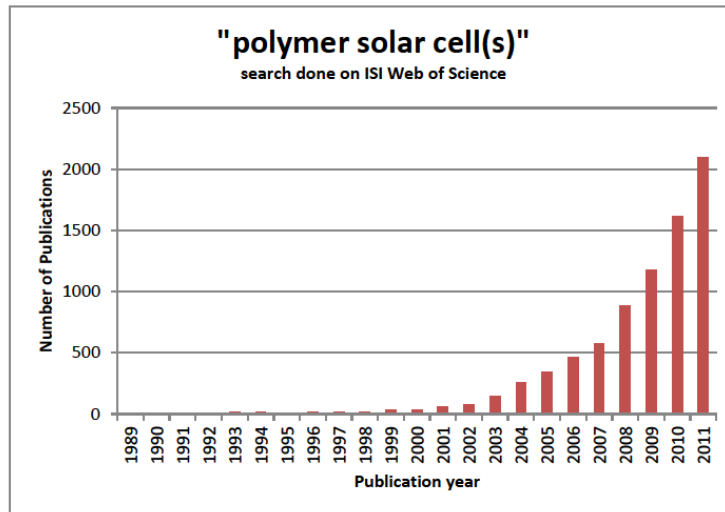
Figure 22: Number of publications per year contributing to the subject of
"polymer solar cell(s)"

Carbon nanotubes have already been used in organic photovoltaics, both as a transparent conducting layer and as an additive to improve performance. The methods I have presented for spraying carbon nanotubes and infiltrating polymer are applicable to use in photovoltaics, and in Appendix 3 I present some preliminary work toward building a photovoltaic device using carbon nanotubes.

7. References

1. Baughman, R. H.; Zakhidov, A. A.; de Heer, W. A., Carbon nanotubes - the route toward applications. *Science* **2002,** *297* (5582), 787-792.
2. Villers, D.; Sun, S. H.; Serventi, A. M.; Dodelet, J. P.; Desilets, S., Characterization of Pt nanoparticles deposited onto carbon nanotubes grown on carbon paper and evaluation of this electrode for the reduction of oxygen. *Journal of Physical Chemistry B* **2006,** *110* (51), 25916-25925.
3. Guangyong, L.; Liming, L., Carbon Nanotubes for Organic Solar Cells. *Nanotechnology Magazine, IEEE* **2011,** *5* (3), 18-24.
4. Hu, L.; Hecht, D. S.; Gruner, G., Percolation in transparent and conducting carbon nanotube networks. *Nano Letters* **2004,** *4* (12), 2513-2517.
5. Kitano, T.; Maeda, Y.; Akasaka, T., Preparation of transparent and conductive thin films of carbon nanotubes using a spreading/coating technique. *Carbon* **2009,** *47* (15), 3559-3565.
6. Jo, J. W.; Jung, J. W.; Lee, J. U.; Jo, W. H., Fabrication of Highly Conductive and Transparent Thin Films from Single-Walled Carbon Nanotubes Using a New Non-ionic Surfactant via Spin Coating. *Acs Nano* **2010,** *4* (9), 5382-5388.
7. Majumder, M.; Rendall, C.; Li, M.; Behabtu, N.; Eukel, J. A.; Hauge, R. H.; Schmidt, H. K.; Pasquali, M., Insights into the physics of spray coating of SWNT films. *Chemical Engineering Science* **2010,** *65* (6), 2000-2008.
8. Tenent, R. C.; Barnes, T. M.; Bergeson, J. D.; Ferguson, A. J.; To, B.; Gedvilas, L. M.; Heben, M. J.; Blackburn, J. L., Ultrasmooth, Large-Area, High-Uniformity, Conductive Transparent Single-Walled-Carbon-Nanotube Films for Photovoltaics Produced by Ultrasonic Spraying. *Advanced Materials* **2009,** *21* (31), 3210-+.
9. Byrne, M. T.; Gun'ko, Y. K., Recent Advances in Research on Carbon Nanotube–Polymer Composites. *Advanced Materials* **2010,** *22* (15), 1672-1688.
10. Pei, L.; Abbott, J.; Zufelt, K.; Davis, A.; Zappe, M.; Decker, K.; Liddiard, S.; Vanfleet, R.; Linford, M. R.; Davis, R., Processing of Thin Carbon Nanotube-Polyimide Composite Membranes. *Nanoscience and Nanotechnology Letters* **2011,** *3* (4), 451-457.
11. Moore, V. C. Single walled carbon nanotubes: Suspension in aqueous/surfactant media and chirality controlled synthesis on surfaces. Dissertation, Rice University, 2005.
12. Kim, K. S.; Bae, D. J.; Kim, J. R.; Park, K. A.; Lim, S. C.; Kim, J. J.; Choi, W. B.; Park, C. Y.; Lee, Y. H., Modification of electronic structures of a carbon nanotube by hydrogen functionalization. *Advanced Materials* **2002,** *14* (24), 1818-1821.
13. Strano, M. S.; Moore, V. C.; Miller, M. K.; Allen, M. J.; Haroz, E. H.; Kittrell, C.; Hauge, R. H.; Smalley, R. E., The role of surfactant adsorption during ultrasonication in the dispersion of single-walled carbon nanotubes. *Journal of Nanoscience and Nanotechnology* **2003,** *3* (1-2), 81-86.
14. Hennrich, F.; Wellmann, R.; Malik, S.; Lebedkin, S.; Kappes, M. M., Reversible modification of the absorption properties of single-walled carbon nanotube thin films via nitric acid exposure. *Physical Chemistry Chemical Physics* **2003,** *5* (1), 178-183.
15. (a) Giordani, S.; Bergin, S.; Nicolosi, V.; Lebedkin, S.; Blau, W. J.; Coleman, J. N., Fabrication of stable dispersions containing up to 70% individual carbon nanotubes in a common organic solvent. *Physica Status Solidi B-Basic Solid State Physics* **2006,** *243* (13), 3058-3062; (b) Bergin, S. D.; Nicolosi, V.; Streich, P. V.; Giordani, S.; Sun, Z.; Windle, A. H.; Ryan, P.; Niraj, N. P. P.; Wang, Z.-T. T.; Carpenter, L.; Blau, W. J.; Boland, J. J.; Hamilton, J. P.; Coleman, J. N., Towards Solutions of Single-Walled Carbon Nanotubes in Common Solvents. *Advanced Materials* **2008,** *20* (10), 1876-1881.

16.   Bergin, S. D.; Sun, Z. Y.; Rickard, D.; Streich, P. V.; Hamilton, J. P.; Coleman, J. N., Multicomponent Solubility Parameters for Single-Walled Carbon Nanotube-Solvent Mixtures. *Acs Nano* **2009,** *3* (8), 2340-2350.

17.   Bergin, S. D.; Sun, Z.; Streich, P.; Hamilton, J.; Coleman, J. N., New Solvents for Nanotubes: Approaching the Dispersibility of Surfactants. *The Journal of Physical Chemistry C* **2009,** *114* (1), 231-237.

18.   Spitalsky, Z.; Tasis, D.; Papagelis, K.; Galiotis, C., Carbon nanotube–polymer composites: Chemistry, processing, mechanical and electrical properties. *Progress in Polymer Science* **2010,** *35* (3), 357-401.

19.   Satyanarayana, N.; Rajan, K.; Sinha, S.; Shen, L., Carbon Nanotube Reinforced Polyimide Thin-film for High Wear Durability. *Tribology Letters* **2007,** *27* (2), 181-188.

20.   Lebrón-Colón, M.; Meador, M. A.; Gaier, J. R.; Solá, F.; Scheiman, D. A.; McCorkle, L. S., Reinforced Thermoplastic Polyimide with Dispersed Functionalized Single Wall Carbon Nanotubes. *ACS Applied Materials & Interfaces* **2010,** *2* (3), 669-676.

21.   Ohring, M., *Materials Science of Thin Films*. 2nd ed.; Academic Press: 2001.

22.   Sun, Z.; Nicolosi, V.; Rickard, D.; Bergin, S. D.; Aherne, D.; Coleman, J. N., Quantitative Evaluation of Surfactant-stabilized Single-walled Carbon Nanotubes: Dispersion Quality and Its Correlation with Zeta Potential. *The Journal of Physical Chemistry C* **2008,** *112* (29), 10692-10699.

23.   Sze, S. M., *Semiconductor Devices: Physics and Technology*. 2nd ed.; John Wiley & Sons: 2002.

24.   Dennler, G.; Scharber, M. C.; Brabec, C. J., Polymer-Fullerene Bulk-Heterojunction Solar Cells. *Advanced Materials* **2009,** *21* (13), 1323-1338.

25.   Hoppe, H.; Sariciftci, N., Polymer Solar Cells: Photoresponsive Polymers II. Marder, S.; Lee, K.-S., Eds. Springer Berlin / Heidelberg: 2008; Vol. 214, pp 1-86.

26.   Thompson, B. C.; Fréchet, J. M. J., Polymer–Fullerene Composite Solar Cells. *Angewandte Chemie International Edition* **2008,** *47* (1), 58-77.

27.   Mühlbacher, D.; Scharber, M.; Morana, M.; Zhu, Z.; Waller, D.; Gaudiana, R.; Brabec, C., High Photovoltaic Performance of a Low-Bandgap Polymer. *Advanced Materials* **2006,** *18* (21), 2884-2889.

28.   Peet, J.; Kim, J. Y.; Coates, N. E.; Ma, W. L.; Moses, D.; Heeger, A. J.; Bazan, G. C., Efficiency enhancement in low-bandgap polymer solar cells by processing with alkane dithiols. *Nat Mater* **2007,** *6* (7), 497-500.

29.   Kim, J. Y.; Lee, K.; Coates, N. E.; Moses, D.; Nguyen, T.-Q.; Dante, M.; Heeger, A. J., Efficient Tandem Polymer Solar Cells Fabricated by All-Solution Processing. *Science* **2007,** *317* (5835), 222-225.

30.   McDonald, T. J.; Svedruzic, D.; Kim, Y.-H.; Blackburn, J. L.; Zhang, S. B.; King, P. W.; Heben, M. J., Wiring-Up Hydrogenase with Single-Walled Carbon Nanotubes. *Nano Letters* **2007,** *7* (11), 3528-3534.

31.   Tanaka, Y.; Hirana, Y.; Niidome, Y.; Kato, K.; Saito, S.; Nakashima, N., Experimentally Determined Redox Potentials of Individual (n,m) Single-Walled Carbon Nanotubes. *Angewandte Chemie International Edition* **2009,** *48* (41), 7655-7659.

8. Appendix 1: Bulge testing equation

Starting with the bulge testing equation,

$$\frac{Y}{1-v} = \left(P * \frac{r^2}{4dh} - \sigma \right) * \frac{3r^2}{2h^2},$$

we solve for the pressure P as a function of h, to yield a 3rd order polynomial of the form

$$P(h) = A_1 h + A_2 h^3.$$

A_1 and A_2 are determined by fitting the experimental data for P and h, and then the unknowns

$Y/(1-v)$ and σ can be determined by

$$\sigma = A_1 \frac{r^2}{4d}; \qquad \frac{Y}{1-v} = A_2 \frac{3r^4}{8}.$$

9. Appendix 2: Matlab fitting program

```matlab
clear;  close all;
Filename='300nmSWNTcompositeMoxtek38mm(2).csv'; %Enter filename here

d=300e-9;              %Fill in the measured thickness of film (m)
r=(3.8e-3)/2;          %Fill in the Radius of washer (m)
N=10                   %Fill in the number of data points to drop
                       %from the end of the fit

                       %Program begins here

rawData1=csvread(Filename);      %Reading data file
x=rawData1(:,2);
x=(x-x(1))*1e-6;                 %Converting from microns to meters
y1=rawData1(:,1); ymax=max(y1)
y1=y1*6894.76;                   %Converting pressure from PSI to Pascals

x=x(1:(length(x)-N));
y1=y1(1:(length(y1)-N));

a1=[0,1e9,0];                    %Educated guess at constants
xmin=min(x);                     %[sigma, Y, zero offset]
xmax=max(x);
npts=1001;
dx=(xmax-xmin)/(npts-1);
xplot=xmin:dx:xmax;

option=optimset('TolX',1e-5);
a1=fminsearch(@leastsq,a1,option,x,y1);
                                 %Perform the fit
                                 %The form of the equation you're fitting
                                 %is in the file called funcfit.m

format ShortE;
a1
sigma=a1(1)*r^2/4/d              %Solve for sigma and Y
Y=a1(2)*3*r^4/8/d
zero=a1(3)


string1=char(...                 %Create a label for the graph
    ['Filename = ' Filename],...
    ['Y/(1-v)=' num2str(Y, '%10.2e') ' Pa'],...
    ['Sigma = ' num2str(sigma, '%10.2e') ' Pa'],...
    ['Points discarded at end = ' num2str(N)],...
    ['Highest pressure = ' num2str(ymax) ' PSI'],...
    ['Zero offset = ' num2str(zero*1e6) ' um']...
    )

yplot1=funcfit(a1,xplot);        %Graphing (note: switching x and y axis)
plot(y1/6894.76,x*1e6,'b.',yplot1/6894.76,xplot*1e6,'r-');
ylabel('deflection (um)');
xlabel('Pressure (PSI)');
```

```matlab
title('Pressure data with best fit');
text(max(yplot1/2/6894.76),max(xplot/2*1e6),string1,...
    'HorizontalAlignment','left')




%%% The least squares .m file called by the fitting program
function s=leastsq(a,x,y)
s=sum((y-funcfit(a,x)).^2);




%%%The funcfit .m file called by the fitting program
function f=funcfit(a,x)
f=a(1).*(x-a(3))+a(2)*(x-a(3)).^3;

% f=a*(x-b)+c*(x-b)^3
% b is an offset to account for initial slack in the film
```

10.   Appendix 3: Work towards an organic photovoltaic device

Typical organic photovoltaic devices are currently made by blending a pi-conjugated photosensitive polymer such as poly-3(hexylthiophene) or P3HT with a functionalized fullerene derivative, PCBM.[25]

When conjugated polymers such as P3HT absorb light, an electron is excited from the lowest unoccupied molecular orbital (LUMO) into the highest unoccupied molecular orbital (HOMO) (See Figure 23). This excited state, or bound electron-hole pair, is called an exciton, and generally has a diffusion length between 5-20 nm in the P3HT. If an electron acceptor (such as PCBM) is distributed throughout the polymer, electrons can be transferred into the LUMO of acceptor molecules, and then be carried through conductive networks to an electrode. It is therefore important that the LUMO of the acceptor molecule be lower than the LUMO of the donor (polymer) as shown in Figure 23. An ideal acceptor LUMO should be about 0.3 eV below the LUMO level of the donor molecules.[26] The open circuit voltage of a solar cell is typically correlated to the difference between the HOMO of the donor material and the LUMO of the acceptor.[26]

So far, only derivatives of C60 and C70 have been reported to give highly efficient bulk heterojunction devices, despite the fact that the position of the HOMO and LUMO levels and optical absorption are not ideal.[24] Several molecules have been tried but so far none have matched the efficiency of fullerene devices.[25]

Carbon nanotubes have been used as acceptor molecules with varying results. Small-diameter single wall nanotubes have a high electron mobility and a favorable band gap.[24]
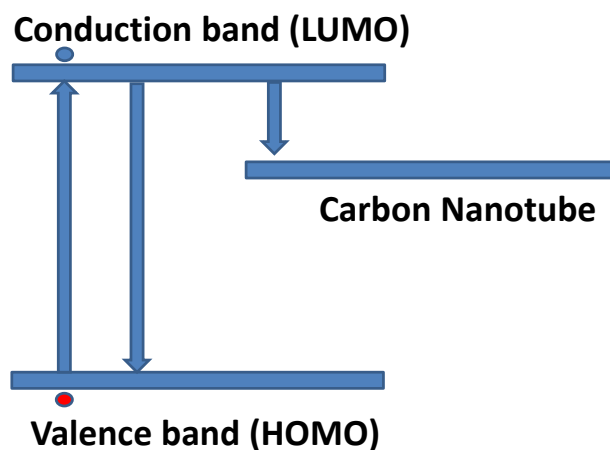
Figure 23: Schematic showing energy levels of
photoactive polymer and carbon nanotube

PCPDTBT (or Poly[2,1,3-benzothiadiazole-4,7-diyl[4,4-bis(2-ethylhexyl)-4H-cyclopenta[2,1-b:3,4-b']dithiophene-2,6-diyl]]) has been shown to be a promising narrow-bandgap photoactive polymer.[27] PCPDTBT has a nearly optimal bandgap of 1.46, and when combined with PCBM and a small amount of alkanedithiols to modify the morphology, it has shown efficiencies of 5.5%.[28] While carbon nanotubes have been combined with other photoactive polymers, to our knowledge carbon nanotubes have not been combined with PCPDTBT to make a photovoltaic device.
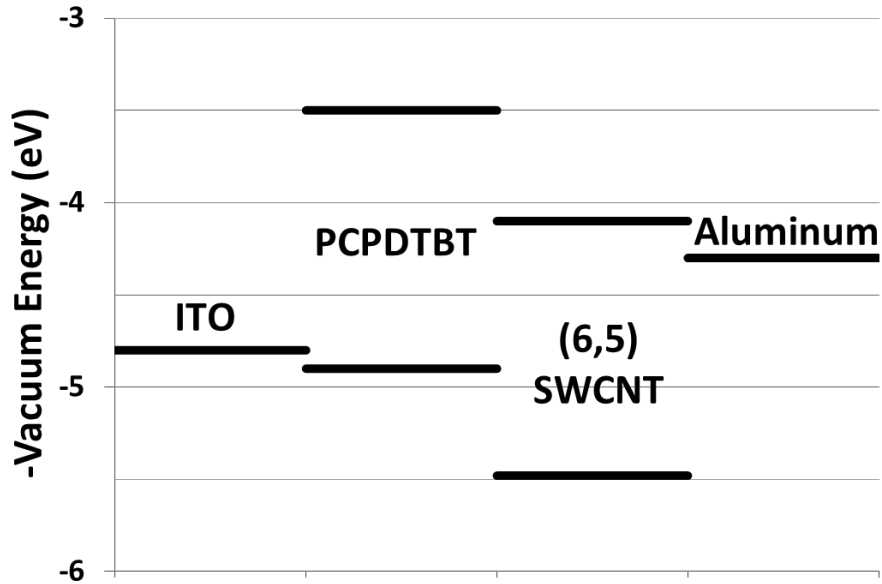
Figure 24: Proposed device using PCPDTBT and (6,5) carbon nanotubes. The energy levels of ITO and PCPDTBT in this figure are from Kim et al.,[29] while values for the (6,5) carbon nanotubes are an average of McDonald et al.[30] and Tanaka et al.[31]

10.1.   Structure for photovoltaic device

One of my long term goals was to build a 3 layer device with a photon absorbing, electron donating polymer top layer, a middle insulating layer with nanotubes passing through it, and an electron accepting nanotube bottom layer. A device like this is shown in Figure 25 a, which in theory could be prepared by spinning a photosensitive polymer onto commercially available indium-tin oxide glass, spraying nanotubes onto the polymer, spinning on polyimide, etching back the polyimide to expose nanotubes, then finally evaporating aluminum to form the back contact. Several problems were encountered with building this proposed structure. It was found that PCPDTBT was soluble enough in NMP that spraying NMP-suspended nanotubes onto a neat film of PCPDTBT destroyed the film, and the PCPDTBT reflowed, forming miniature hillocks (shown in Figure 26).
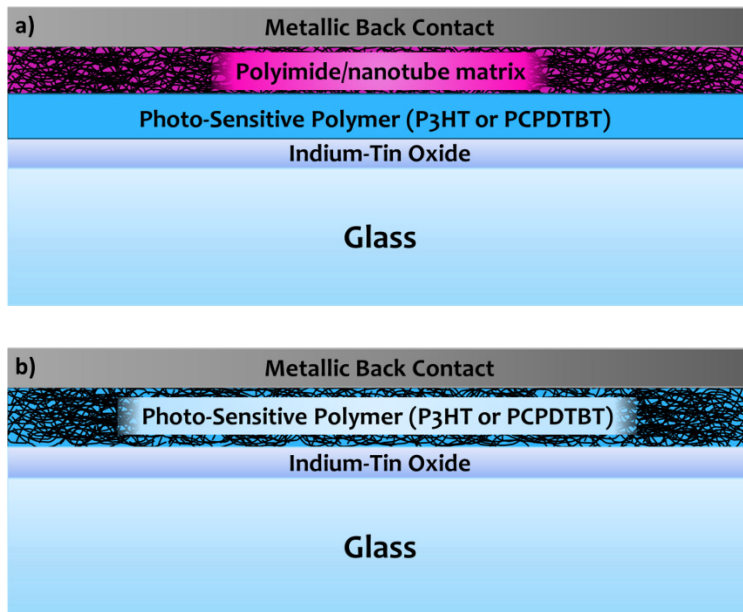
Figure 25: a) Proposed structure for 3 layer device b) Device without middle insulating layer
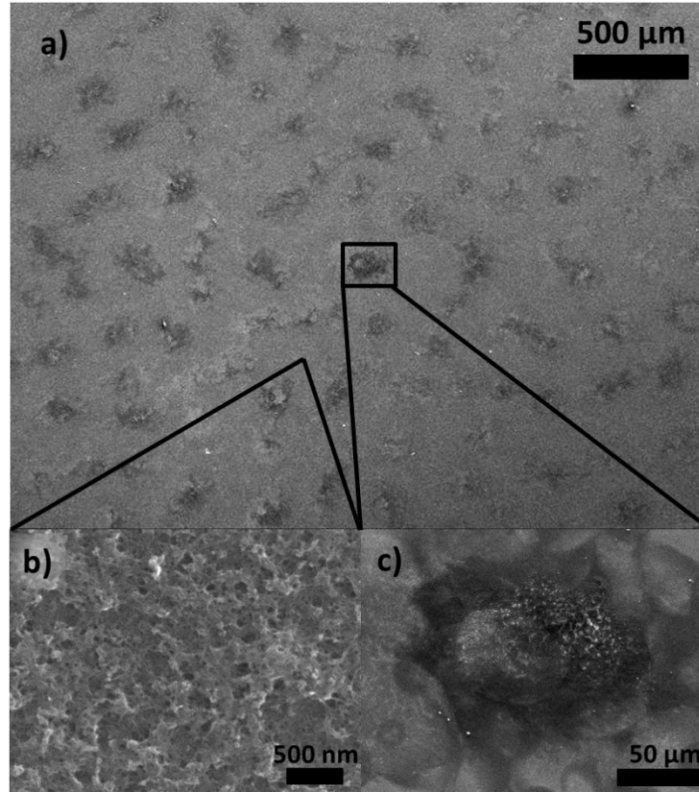
Figure 26: a) SEM image of nanotubes sprayed on a thin film of PCPDTBT b) Zoomed in to show structure of nanotube region c) Zoomed in to show structure of a hillock

I also tried creating the structure in Figure 25 b by spinning PCPDTBT onto a film of nanotubes, etching the film back slightly, as in Figure 21, and then evaporating aluminum contacts. The contacts had a dull appearance compared to aluminum evaporated elsewhere and the films did not produce a detectable voltage when exposed to light. I suspect there may have been problems with the aluminum contact reacting with the PCPDTBT beneath.